Trends in

Applied Sciences Research

ISSN 1819-3579

Academic
Journals Inc.

www.academicjournals.com

Trends in Applied Sciences Research 1 (5): 456-466, 2006
ISSN 1819-3579
© Academic Journals Inc., USA

Modelling and Simulation of a New Micromachined Acoustic Sensor

[1]B. Mezghani, [1]F. Tounsi, [1]S. Smaoui, [2]K. Haboura, [2]S. El-Borgi,
[3]S. Choura and [1]M. Masmoudi
[1]Engineering School of Sfax, ENIS, BP W, 3038 Sfax, Tunisia
[2]Tunisia Polytechnic School, Tunis, Tunisia
[3]Preparatory Institute for Engineering Study of Sfax, 3018 Sfax, Tunisia

Abstract: In this study, we present modelling and simulation results of a new micromachined acoustic sensor. Equation derivation of the variable mutual inductance is summarized. Two attachment structures of the suspended membrane, the I-shaped and L-shaped beams, are modeled and simulated. Using a theoretical mechanical modelling, we get displacement values of 13.11 and 68.82 μm, for the I-shaped and L-shaped beam design, respectively. With a numerical FEM design, displacement values of 12.7 and 63.5 μm were found for the I-shaped and L-shaped beam design, respectively. Using the analogy between acoustic, mechanical and electrical domains, the dynamic behaviour of the microphone is modeled, then simulated and a corner frequency around 200 kHz is found. This same value is found when applying analytical dynamics principles to determine the equations of motion for the suspended membrane. A FEM analysis is conducted in order to validate this theoretical model. This sensor is analyzed for mechanical-thermal noise by modelling the suspended membrane with its mass-spring oscillator diagram. The damping factor is found to be 4×10^{-2} N s m^{-1}, which gives a fluctuating force spectral density of 2.57×10^{-11} N $Hz^{-1/2}$ and an A-weighted sound level of about 38 dB(A) SPL.

Key words: Mechanical modelling, numerical simulations, acoustic modelling, micromachined, acoustic sensor, thermal noise modelling

Introduction

The introduction of MEMS (Micro-Electro-Mechanical Systems) technology has led to many fabrication and integration improvements in the area of micromachined integrated microphones (Pedersen, 1997). Capacitive micromachined microphones are known to have the best sensitivity and offer the best performance (Chen *et al*., 2003; Iguchi *et al*., 2004). However, their integration needs specific materials and fabrication technology.

The evolution of high performance new generation silicon integrated sensors based on micromachining technology has focalized, until now, on the need for monolithic integration of the sensor with its controlling electronics (Savalli *et al*., 2004; Latorre *et al*., 2004). This is using the standard CMOS Integrated Circuit fabrication technology, which is quite developed. Therefore, silicon integrated sensors can be produced reliably, economically (in the high volumes required by today's fastest growing markets) and with similar characteristics. This monolithic integration will increase performances, miniaturize the system, increase the sensitivity and in particular decrease noise, due to the reduction of interconnections parasitic capacitance.

The state-of-the art CMOS micromachined inductive microphone is one example of a monolithically integrated acoustic sensor. The mode of operation of this new acoustic sensor is based on the variation of mutual inductance between an external fixed inductor and an internal suspended inductor. This internal inductor is designed on a 1.4×1.4 mm^2 suspended membrane attached to the substrate with 4 beams.

Corresponding Author: B. Mezghani, Engineering School of Sfax, ENIS, BP W, 3038 Sfax, Tunisia

The Inductive Microphone Structure

The structure and a cross sectional views of the inductive microphone are shown in Fig. 1. The fixed external inductor L1 is fabricated on top of the Silicon substrate. The internal inductor L2 is designed on top of a suspended membrane attached to the substrate with either the I-shaped beam (simple cantilever) or the L-shaped beam (folded-flexure). The microphone is normally mounted on a housing to solidify and support the whole structure. This housing is also required to create the enclosed volume under the suspended membrane (back chamber). Moreover, the housing is necessary to generate the differential sound pressure over the suspended membrane.

In our design, the acoustic holes or membrane openings are modeled by N' squares with side length equal to the distance e separating the beam from the substrate. The number of acoustic square holes N' is given by:

$$N' = 4\frac{3L-16e}{e} \tag{1}$$

These acoustic holes are necessary in order to allow the air to flow in and out of the back chamber, when the suspended membrane moves according to the applied acoustic sound pressure.

Other than the CMOS compatibility and the elimination of parasitic capacitances, our design does not have the possibility of serious damping. This damping is quite possible in other conventional capacitive designs, which results from the small distance between the two capacitance plates (air gap). The damping will result in a low roll-off frequency and sensitivity. Since in our design the air gap will be large (the substrate thickness), we will neglect the damping effect in our modelling and simulations.

The layout and fabrication of this acoustic sensor are under study in a CMOS compatible process using a 0.8 μm technology. The biggest problem that we have to solve is the release of the suspended membrane (1.4×1.4 mm^2) using the standard technology steps. To get the maximum induced output voltage, the internal coil (50 turns) should be fabricated at the periphery of the suspended membrane. This says that we will have a large empty surface at the center of the suspended membrane. Etch holes, having the form of a 45° line (etch line), will be added in this large empty surface. The width of the etch line is fixed by the minimum distance allowed by the technology design rules. However, their length is limited by the internal coil layout. Each etch line will release a form of a rectangle below it.

Since these etch lines have very small dimensions compared to the distance e, they will not have an effect on the overall performance of the sensor. In addition, since we have a large empty surface in the suspended membrane center, these etch lines will not affect the deposition of the internal coil.

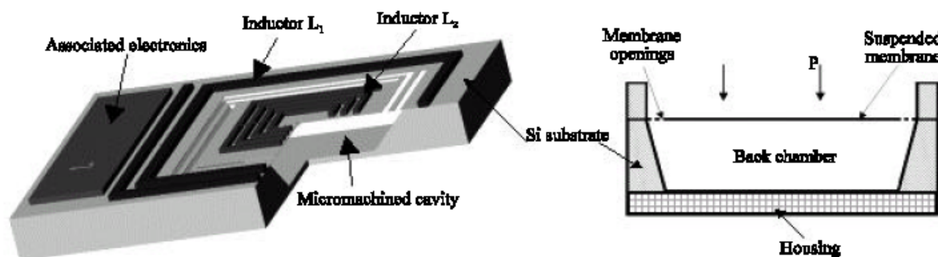

Fig. 1: The inductive microphone structure and cross sectional view

Inductors Total and Mutual Inductances Calculations

Because of the simple layout and symmetry properties of the square geometry, the square spiral inductor will be used for both internal and external inductors. Using a physical model based on the summation of average segment interaction of mutual inductances present in the structure, the total inductance Ls of a square spiral inductor is given by (Tounsi, 2003; Jenei *et al*., 2002):

$$\begin{aligned} L_s = \frac{\mu_0 l}{2\pi}\Bigg[& \ln\left(\frac{l}{n(w+t)}\right) - 0.2 - 0.47n \\ & +(n-1)\left[\ln\left(\sqrt{1+\left(\frac{l}{4nd^+}\right)^2}+\frac{l}{4nd^+}\right)-\sqrt{1+\left(\frac{4nd^+}{l}\right)^2}+\frac{4nd^+}{l}\right]\Bigg] \end{aligned} \tag{2}$$

With

$$d^+ = (w+s)\frac{(3n-2N-1)(N+1)}{3(2n-N-1)} \tag{3}$$

Where μ_0 is the vacuum permeability, N is the integer part of the number of turns n and d^+ is the average distance for the constituting factor of positive mutual inductance. The total length, width, spacing and thickness of the spiral are l, w, s and t, respectively. The induced voltage in the internal inductor L2 is proportional to the mutual inductance between the two inductors and the current flowing in the external inductor. The mutual inductance, M_{tot} is formed by three terms:

$$M_{tot} = M_{L1} + M_{L2} + M_{L1\rightarrow L2}$$

Where M_{L1} and M_{L2} are the constant own mutual inductances of inductor L1 and inductor L2, respectively. The third term in the above equation is the mutual inductance of interest. It will be calculated using the Greenhouse algorithm which is based on summing the mutual inductance of each individual segment interactions. In our case, the calculations are done in a recursive manner between each individual segment of the external inductor and the segments of the internal inductor. The expression of the mutual inductance benefits in simplicity from the symmetry properties of the square geometry. In Fig. 2, we show the layout of two distant segments of inductors 1 and 2, used to find the mutual inductance. Using the Greenhouse formula given in (Greenhouse, 1974) and after simplifications, the mutual inductance equation is found to be given by:

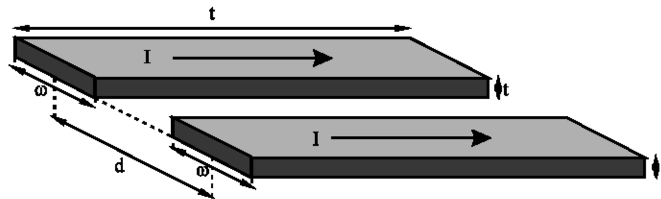

Fig. 2: Layout of two distant segments of internal and external inductors

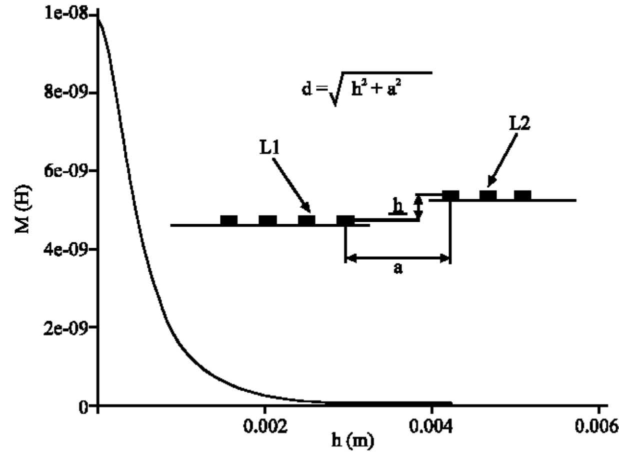

Fig. 3: Mutual inductance variations versus relative displacement

$$M(l,d) \approx \frac{\mu_0 l}{2\pi}\left[\ln\left(\sqrt{1+\left(\frac{l\exp(\frac{w^2}{12d^2})}{d}\right)^2}+\frac{l\exp(\frac{w^2}{12d^2})}{d}\right)-\sqrt{1+\left(\frac{d}{l\exp(\frac{w^2}{12d^2})}\right)^2}+\frac{d}{l\exp(\frac{w^2}{12d^2})}\right] \quad (4)$$

The mutual inductance variation, as a function of the relative displacement h between inductors 1 and 2, is given in Fig. 3. We clearly see that the mutual inductance is linear for the displacement values of interest.

Suspended Membrane Displacement

Two different types of suspended membrane attachments were modeled and simulated, the I-shaped beam (simple cantilever) and the L-shaped beam (folded-flexure).

Many other attachment types were considered, but they either give an imbalanced displacement (torsion), or no significant displacement. Much closer inductors are obtained using the I-shaped beam membrane attachments. But the L-shaped beam attachments offer greater membrane elasticity.

Since the suspended membrane has multiple layers of different material (oxide and metal), its mass should be computed using the following equation:

$$m = \sum_i d_{i_n} \times V_{i_n} \quad (5)$$

Where d_i is the layer material density and V_i is its respective volume. Knowing the densities of the oxide and metal, the membrane surface of 1.4×1.4 mm^2 and the volumes of the different membrane layers, we can compute the mass of the system. We found that the mass is approximately equal to 22 μg.

The displacement value h was determined with a mechanical modelling done on the suspended membrane subjected to its weight and to a static pressure of 1 Pa. The side length of the suspended membrane used was 1.4 mm. All other elements (thickness, spacing, width, length) for both the suspended membrane and attachment beams were defined according to the design rules imposed by the technology used. The problem studied was the dynamics of a square rigid plate supported by 4 beams which are modeled by springs having specific stiffness k. The plate displacement is given by:

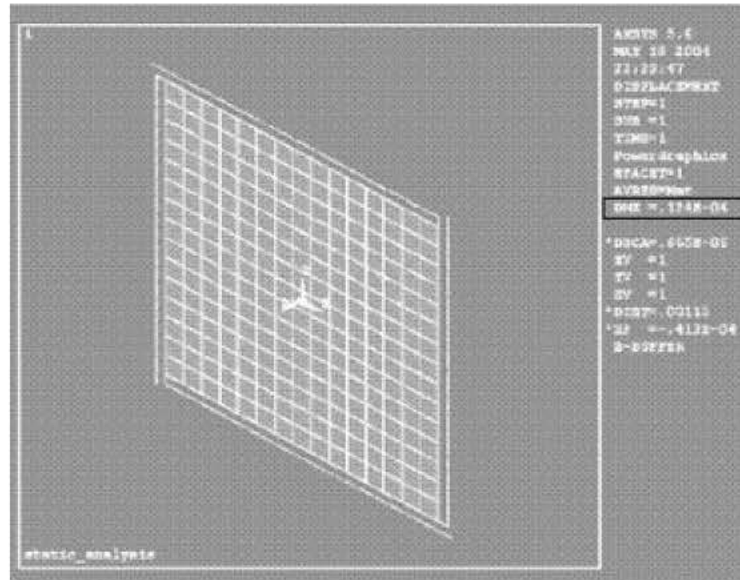

Fig. 4: Suspended membrane displacement with the I-shaped beam attachments

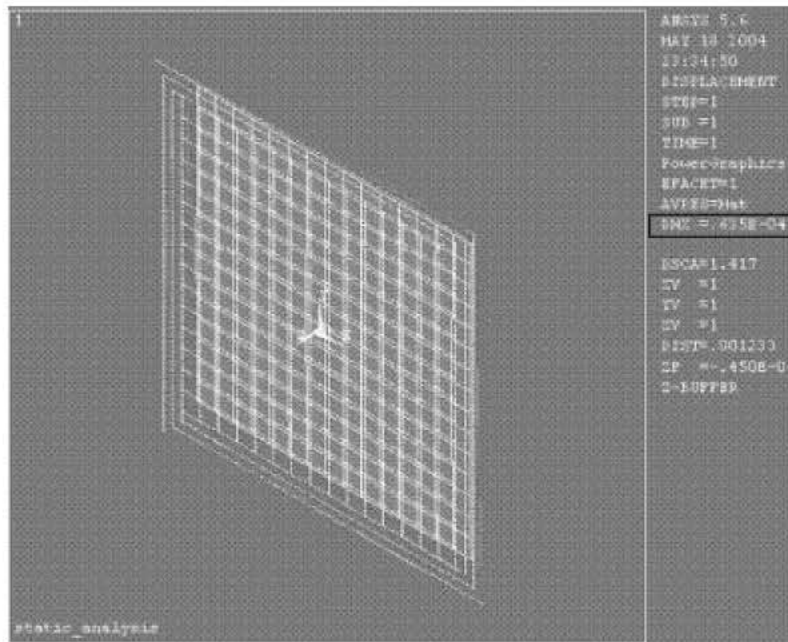

Fig. 5: Suspended membrane displacement with the L-shaped beam attachments

$$h = \frac{Pa^2 + mg}{4k} \tag{6}$$

Where P is the acoustic pressure value, a and m are the side length and mass of the membrane, respectively.

The I-shaped and L-shaped beam spring stiffness, k_I and k_L, are given by:

$$k_I = \frac{3EI}{L^3} \quad \text{and} \quad k_L = \frac{6EI}{7L^3} \tag{7}$$

Where E is the Young's modulus, I is the moment of inertia and L is the total length of the beam.

Using this mechanical modelling, we get displacement values of 13.11 and 68.82 μm, for the I-shaped and L-shaped beam designs, respectively. These values obtained using theoretical models were compared with a numerical FEM design using the Ansys software (Mezghani *et al*., 2006). Displacement values of 12.7 and 63.5 μm were found for the I-shaped and L-shaped beam design, respectively. The simulation results are shown in Fig. 4 and 5.

We clearly see that the displacement obtained with the L-shaped beam attachments is much more important than that obtained with the I-shaped beam attachments. Since the induced voltage in L2 is directly proportional to the relative displacement between the outer and inner inductances, therefore, only the L-shaped beam structure will be studied.

Dynamic Behaviour of the Inductive Microphone Structure

Using the Analogy Between the Three Physical Domains

The microphone is an electro-mechanical-acoustic transducer that transforms acoustical energy into electrical energy. Therefore, to understand the quasi static properties of such a device, we have to solve a problem, which is coupled between the three different physical domains. One common way to approach this problem is to use the analogy that exists between these three domains. As a consequence, all acoustic and mechanical properties of the microphone can be defined as elements (resistors, capacitors and coils) in an equivalent electrical circuit. When applying the analogy between the different domains described above, a linear circuit model of the inductive microphone can be derived. The cross sectional view of the basic structure of the inductive microphone is shown in Fig. 1. It consists of a suspended membrane, which separates the surroundings from the back chamber. When a surrounding acoustic pressure is applied, a pressure difference appears with the back chamber, causing the suspended membrane to deflect.

Considering this coupled system, the following dynamic effects must be included:

- Resistance and mass due to radiation from the membrane
- Compliance and mass of the membrane
- Resistance and mass of the air in the membrane openings
- Compliance of the air in the back chamber

Since the microphone dimensions are small compared to the smallest wavelength of interest (λ at 20 kHz ≈ 17 mm), the dynamics of the entire inductive microphone system can be approximated by a linear circuit model that is shown in Fig. 6 (Mezghani *et al*., 2004). The mechanical components on which equal forces act are connected in parallel and components having the same velocity are connected in series.

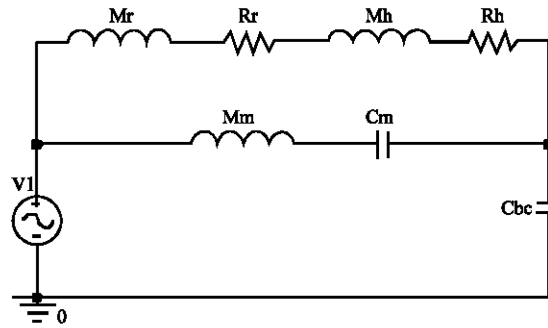

Fig. 6: Equivalent linear mechanical circuit of the inductive microphone

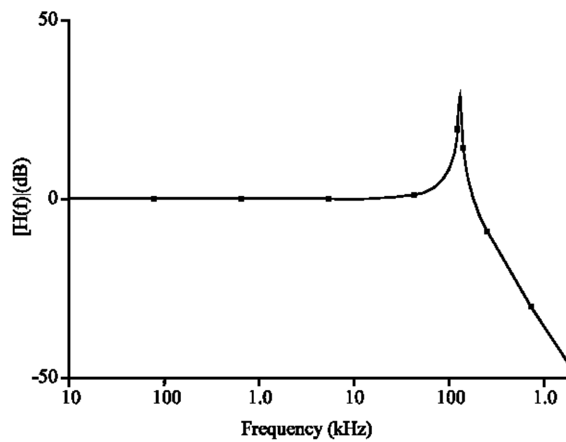

Fig. 7: Theoretical Bode diagram of the microphone dynamic response

The equivalent linear mechanical circuit of the integrated inductive microphone shown in Fig. 6 has been implemented and simulated using the SPICE circuit simulator. The Bode diagram of the gain is plotted in Fig. 7. The corner frequency was found to be around 200 kHz.

Using Theoretical and Numerical Modelling

To verify the above study and natural frequency value found, both theoretical and numerical modelling of the microphone dynamics were carried out.

The theoretical modelling consisted in using analytical dynamics principles in order to derive the equations of motion for the suspended membrane. We supposed that the acoustic pressure is harmonic and normal to the plate ($P(t) = P_0 \sin\omega t$) and we neglect the damping. Then, the resolution of the Lagrange's equations, using the expressions for the kinetic and potential energies and the generalized forces, gave a system of non-linear equations of motion for the membrane. This system of equations was first linearized and then solved for the natural frequencies. The equation of the natural frequency of interest was equal to:

$$\omega^2 = \frac{6k}{abm} \tag{8}$$

Where a and b are the side lengths of the suspended membrane. This discrete parameter model of the membrane dynamics gave a natural frequency value of 199 kHz.

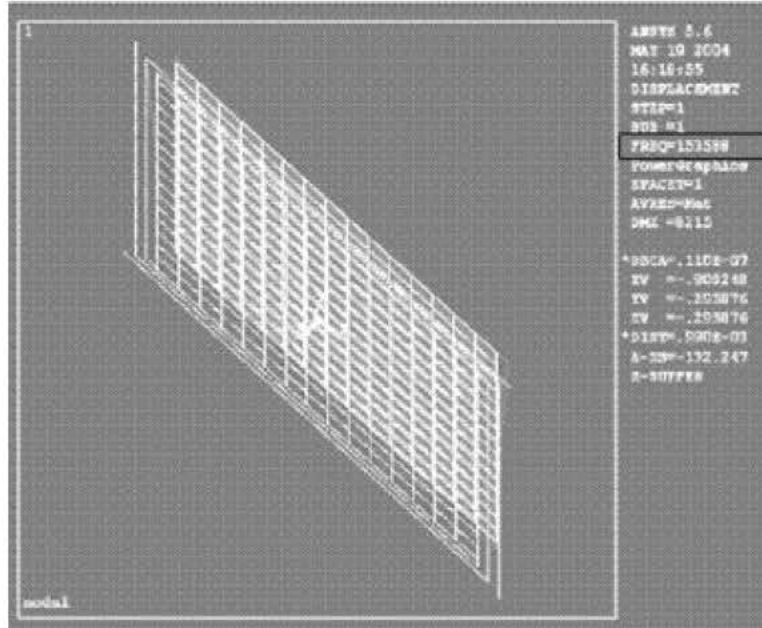

Fig. 8: Modal analysis for suspended membrane natural frequency

A numerical FEM analysis was then conducted in order to validate the theoretical model. The simulation result is shown in Fig. 8. A value of 154 kHz was found for the natural frequency of interest for the suspended membrane. This states that both the meshing and modelling used for the L-shaped beam attachments need further refinement. But, we can safely validate the fact that the microphone response to an audible sound would be linear.

Mechanical-thermal Noise Modelling

Mechanical-thermal noise results from molecular agitation, which can be the limiting noise component, if the sensor is intended for low-level signals and when the sensor technology is pushed to the limit of its sensitivity. The component agitation is caused by molecular collisions from a surrounding gas and the agitation is directly proportional to the fluid's viscosity. Since the signal-to-noise ratio is proportional to the mass, then reducing dimensions in MEMS tiny sensors will increase the Brownian noise.

The thermodynamically proper equation of motion for the displacement z of a damped harmonic oscillator with mass m, spring constant k and mechanical resistance R (Damping factor), is given in (Gabrielson, 1993) by:

$$m\frac{d^2z}{dt^2} + R\frac{dz}{dt} + kz = f_n(R,t) \tag{9}$$

The Nyquist's relation gives the spectral density of the fluctuating force related to any mechanical resistance:

$$F = \sqrt{4k_B TR} \qquad [N \cdot Hz^{-1/2}] \tag{10}$$

The fluctuation pressure p related to any acoustic resistance $R_{ac} = \frac{R}{S^2}$, where S is the area of the active face, is given by:

$$p = \sqrt{4k_B T R_{ac}} \qquad [\mathrm{Pa} \cdot \mathrm{Hz}^{-1/2}] \tag{11}$$

Where k_B is the Boltzmann constant (1.38×10^{-23} J K^{-1}) and T is the absolute temperature.

We clearly see that the fluctuation pressure is directly proportional to the square root of the mechanical resistance (damping factor). This spectral density is a direct physical analogy of Johnson noise in an electrical resistance. This should be the case, since Johnson noise is produced by scattering of free electrons by mechanical thermal vibration of the conductor's solid lattice.

In (Gabrielson, 1993), the above mechanical-thermal noise analysis and equations were used as a starting point for the derivation of the analytical equation for the damping factor *R*. The analysis done and equations found were only for integrated micromachined accelerometers and for capacitive micromachined acoustic and vibration sensors. All developed equations are as a function of the capacitance plates spacing. However, this variable does not exist in our system since we have only one suspended elastic membrane. Therefore, we have to develop and apply a new analysis for our system to find its damping factor, which is the starting point of any mechanical-thermal noise modelling calculation. This new analysis is detailed in the next sub-section.

Application to the Inductive Microphone

The analysis which will be applied in this section is based on natural frequency and equivalent mass values of the system (suspended membrane). In the inductive microphone pressure sensor, the moving mass (suspended membrane) is directly exposed to the incident acoustic pressure and the displacement of this mass is measured. In Fig. 9, we give a cross sectional view of the inductive microphone with the incident acoustic pressure applied on top of the suspended membrane. Next to it, the schematic diagram including displacement coordinate and applied force is drawn (Mezghani *et al*., 2005).

The suspended mass m moves relative to the substrate, when the suspended membrane is exposed to an acoustic force F. This relative displacement is translated to an induced electrical output signal.

Though the system shown in Fig. 9 is an approximation of the behaviour of a real device, it gives us an easily solvable second order system (suspended membrane). This system's behaviour can be summarized with the following equation:

$$\frac{d^2z}{dt^2} + 2D\omega_n \frac{dz}{dt} + \omega_n^2 = a \tag{12}$$

Where

$$\omega_n = \sqrt{\frac{k}{m}} \qquad D = \frac{R}{2m\omega_n} \tag{13}$$

Equation (13) will be the starting points for our design.

With ω_n (natural frequency of the system) and D (damping coefficient), we can relate mass m, spring constant k and damping factor R to each other.

The natural frequency of the suspended membrane, around 200 kHz, was already found in section 5.

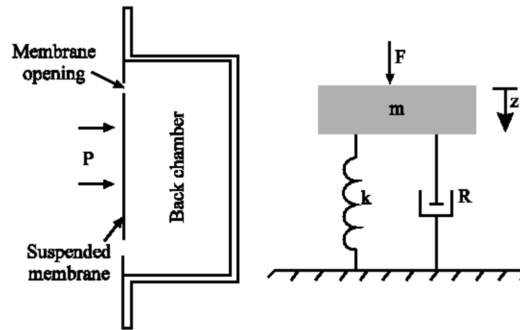

Fig. 9: Cross sectional view of the inductive microphone with its mass-spring oscillator schematic diagram

Our second limitation is that, we want our device to be critically damped. This is because when the system is critically damped, it has the least amplitude distortion and the output follows the input over the widest frequency range. This limitation says that D = 0.707 (Selvakumar, 1997).

Here, the only missing mechanical parameter is the mass of the suspended membrane which was found to be approximately equal to 22 μg.

Then, using Eq. 13, the damping factor R and the acoustic resistance R_{ac} are equal to:

$$R = 4 \times 10^{-2}\ \text{N. s. m}^{-1};\ Rac = 2 \times 10^{4}\ \text{N. s. m}^{-5}$$

This gives a spectral density of the fluctuating force F and the fluctuation pressure p of:

$$F = 2.57 \times 10^{-11}\ \text{N. Hz}^{-½};\ p = 13\ \mu\text{Pa. Hz}^{-½}$$

If the microphone is intended to be used in a system for human communication, it should be rated against the performance of the human ear. Then, the above noise pressure spectral density corresponds to an A-weighted sound level of about 38 dB(A) SPL. This was computed using the equivalent noise bandwidth of the A-weighting function which is about 15 kHz.

In comparison, the ambient noise level ranges from 25 to 30 dB(A) SPL in a quiet recording studio (Anderson, 1989) and from 30 to 50 dB(A) SPL in a quiet residential area (Kinsler *et al*., 1982). Consequently, our microphone is well suited for recording low-level signals in quiet environments.

Conclusions

The inductive microphone is proposed as a new structure of a monolithic CMOS integrated micromachined acoustic sensor.

The equations of total and mutual inductances of the inductors were derived. Two different attachment structures of the suspended membrane were studied. With a theoretical mechanical modelling on the suspended membrane, we get displacement values of 13.11 and 68.82 μm, for the I-shaped and L-shaped beam design, respectively. With a numerical FEM modelling, displacement values of 12.7 and 63.5 μm were found for the I-shaped and L-shaped beam design, respectively.

By using the analogy that exists between the acoustic, mechanical and electrical domains, the dynamic behaviour of the complete microphone structure was modeled. The electrical circuit model of the inductive microphone was derived and simulated. The simulation showed that the microphone has a corner frequency around 200 kHz. This same value was also found with a theoretical mechanical modelling done on the suspended membrane. A numerical FEM modelling and simulation was conducted in order to validate this theoretical model.

Our new acoustic sensor was analyzed for mechanical-thermal noise by modelling the suspended membrane with its mass-spring oscillator diagram. The damping factor of this system was found to be 4×10^{-2} N s m^{-1}, which gave a spectral density fluctuating force of 2.57×10^{-11} N Hz$^{-1/2}$ and an A-weighted sound level of about 38 dB(A) SPL. It was then concluded that our microphone is well suited for sensing low-level signals.

References

Anderson, H.L., 1989. Ed., A Physicist's Desk Reference. Am. Inst. Physics, New York.

Chen, J., L. Liu, Z. Li, Z. Tan, Y. Xu and J. Ma, 2003. On the single-chip condenser miniature microphone using DRIE and backside etching techniques in Sensors and Actuators. A: Physical, 103: 42-47.

Gabrielson, T.B., 1993. Mechanical-thermal noise in micromachined acoustic and vibration sensors. In IEEE Trans. Electron Devices, pp: 903-909.

Greenhouse, H.M., 1974. Design of planar rectangular microelectronic inductors. In IEEE Trans. Parts, Hyb. Packag, 10: 101-109.

Iguchi, Y., T. Tajima, M. Goto, M. Iwaki, A. Ando, K. Tanioka, F. Takeshi, S. Matsunaga and Y. Yasuno, 2004. New fabrication process for high-performance silicon condenser microphone with monocrystalline silicon diaphragm and backplate. In Proceedings of the 17th IEEE International Conference on Micro Electro Mechanical Systems.

Jenei, S., B. Nauwelaers and S. Decoutere, 2002. Physics-based closed-form inductance expression for compact modeling of integrated spiral inductors. In IEEE J.S.S.C., 37: 77-80.

Kinsler, L.E., A.R. Frey, A.B. Coppens and J.V. Sanders, 1982. Fundamentals of Acoustics. 3rd Edn., Wiley, New York.

Latorre, L., V. Berouille and P. Nouet, 2004. Design of CMOS MEMS based on mechanical resonators using a RF simulation approach. In IEEE Trans. C.A.D of I.C. and Syst., 23: 962-967.

Mezghani, B., F. Tounsi, S. Smaoui, M.B. Jallouli, N. Ghamgui and M. Masmoudi, 2004. Modeling of integrated micromachined inductive microphone. In Proceedings of the Joint Japan-Tunisia Workshop on Computer Systems and Information Technology (JT-CSIT'04), July 9-10, Tokyo, Japan, pp: 7-9.

Mezghani, B., F. Tounsi, S. Smaoui, M.B. Jallouli and M. Masmoudi, 2005. Mechanical-thermal noise in CMOS micromachined inductive microphone. In Proceedings of the IEEE International Conference on Electronics, Circuits and Systems (IEEE ICECS 2005), December 11-14, Tunisia, pp: 37-40.

Mezghani, B., K. Haboura, F. Tounsi, S. Smaoui, S. El-Borgi, S. Choura and M. Masmoudi, 2006. Theoretical and Numerical modeling of a CMOS micromachined acoustic sensor. Accepted for publication in Proceedings of the 1st International Conference on Design and Test of Integrated Systems in Nanoscale Technology (IEEE DTIS'06), 5-7 September, 2006, Tunisia.

Pedersen, M., 1997. A polymer condenser microphone realized on silicon containing preprocessed integrated circuits. Ph.D Thesis, University of Twente, the Netherlands.

Savalli, N., S. Baglio, S. Castorina, V. Sacco and C. Tringali, 2004. Integrated CMOS dew point sensors for relative humidity measurement. In Proceedings of the SPIE 11th Annual International Symposium on Smart Structures and Materials, California USA.

Selvakumar, A., 1997. A multi-functional silicon micromachining technology for high performance microsensors and microactuators. Ph.D Thesis, Univ. Michigan.

Tounsi, F., 2003. Contribution à l'Etude et la conception d'un microphone inductif MEMS. M.Sc. Thesis, Engineering School of Sfax, Tunisia.